

Development of *in situ* Electrochemical Small-Angle Neutron Scattering (eSANS) for Simultaneous Structure and Redox Characterization of Nanoparticles

Vivek M. Prabhu^{a*}, Vytas Reipa^a,
Adam J. Rondinone^b, Eric Formo^b and Peter V. Bonnesen^b

^aMaterial Measurement Laboratory, National Institute of Standards and Technology,
Gaithersburg, Maryland 20899, USA

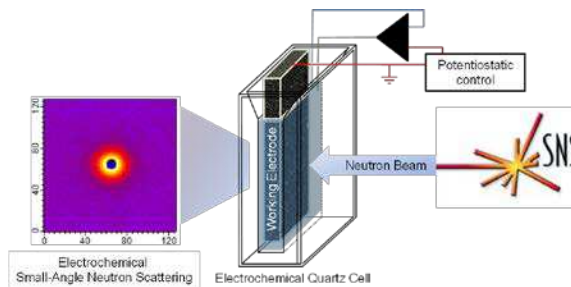
^bCenter for Nanophase Materials Sciences, Oak Ridge National Laboratory,
Oak Ridge, Tennessee 37831, USA

*vprabhu@nist.gov

An *in situ* electrochemical small-angle neutron scattering (eSANS) method was developed to measure simultaneously the redox properties and size, shape and interactions of solution-dispersed nanomaterials. By combining multi-step potentials and chronocoulometry readout with SANS, the structure and redox properties of engineered nanomaterials are followed in one experiment. Specifically, ZnO nanoparticles were examined as dilute dispersions in pH buffered deuterium oxide solutions under negative electrode potentials. The ZnO disk-shaped nanoparticles undergo an irreversible size transformation upon reduction at the vitreous carbon electrode. The decrease in average nanoparticle size near a current maximum shows the reduction reaction from ZnO to Zn occurs. The eSANS method provides nanometer scale sensitivity to nanoparticle size and shape changes due to an electrochemical reaction that is crucial to understand in energy, healthcare, and other applications.

Introduction

The oxidation and reduction (redox) properties of nanomaterials are crucial for catalysis, energy applications, medical contrast imaging and therapy applications and personal care products. In many cases the nanomaterials must undergo hazard assessment for risks caused by a multitude of biosystem exposure paths. For instance, nanomaterials may cause oxidative stress by generating reactive-oxygen species (1-3). Optical spectroscopy analysis of molecules and nanomaterials undergoing redox reactions quantifies the electron transfer and energetics of the reaction via potential control and are the most common analytical techniques employed for this purpose (4). However, with conjugation to organic ligands and smaller, well-defined particle sizes, engineered nanomaterial redox characterization would benefit by techniques that provide nanometer sensitivity to nanoparticle size, shape and ligand structure. In order to address this challenge, an *in situ* electrochemical small-angle neutron scattering (eSANS) method was demonstrated to measure, simultaneously, the redox properties and correlation length



of solution-dispersed nanomaterials during a slow linear potential sweep (5). The application of scattering techniques brings direct size and structure characterization complementing established spectroelectrochemical methods that are sensitive to absorbance characteristics.

In the present development, multi-step potentials and chronocoulometry readout with spallation SANS were applied to follow the structure, pair-wise interactions and redox properties of solution dispersed engineered nanomaterials simultaneously in one experiment. Specifically, ZnO nanoparticles were examined as dilute dispersions in pH buffered deuterium oxide solutions under negative electrode potentials. The ZnO disk-shaped nanoparticles undergo an irreversible size transformation upon reduction at the vitreous carbon electrode. The structure of the dispersion was characterized within the potential range, corresponding to the reduction of the bulk ZnO according to Pourbaix diagram (6), Eq. 1.



Experimental

ZnO disk-like nanoparticle synthesis: 5.5 g of zinc acetate were hydrolyzed in 50 mL of methanol using 0.2 g of solid KOH. The solution was stirred at 85 °C for 48 h and precipitated with centrifugation. The precipitate was washed several times in pure ethanol. Nanoparticles were then solvent exchanged for deuterium oxide by three successive steps of centrifugation and redispersion by sonication. This left a stable concentrated ZnO dispersion in deuterium oxide. Solutions for eSANS were made by mixing the ZnO dispersion with deuterium oxide phosphate buffer to achieve a 25 mmol/L potassium phosphate pH 7 solution. The zeta potential (Malvern Nano ZS) was $-45.1 \text{ mV} \pm 5.6 \text{ mV}$ in this buffer. The ZnO surface groups initially have acetate ion functionality; however, after purification and dispersion in phosphate buffer it is likely the acetate groups are replaced by the divalent phosphate ion leading to charge reversal as observed by zeta potential. TEM (**Figure 1**) confirms the particle shape and size (10.4 ± 2.8) nm radius.

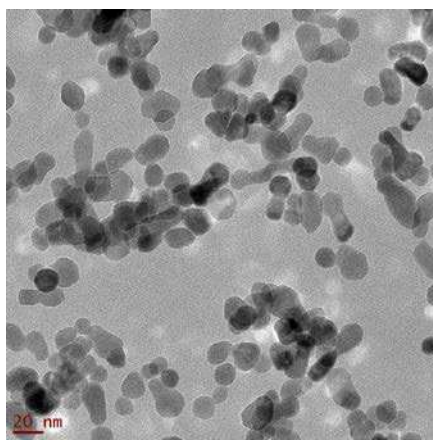


Figure 1. TEM of bare ZnO disk-like nanoparticles. Scale bar of 20 nm at lower left.

Small-angle neutron scattering (SANS) measurements were performed on the BL-6 extended Q-range SANS instrument at the Spallation Neutron Source, Oak Ridge National Laboratory, Oak Ridge, Tennessee. At the Spallation Neutron Source, hydrogen ions are accelerated to 1 GeV and stripped of their electrons, the resulting

protons are accumulated in a storage ring with energy 895.5 MeV. These protons collide with a moderated liquid mercury target at a repetition rate of 60 Hz generating intense pulses of neutrons guided to various instruments. The SANS instrument was operated in a frame-skipping mode whereby the initial broad wavelength distribution of neutrons pass through 4 synchronized choppers rotating at 30 Hz permitting continuous frames of neutrons with wavelength (2 to 5.4) Å and (8.9 to 12.3) Å. The neutrons that pass through the choppers are scattered by the sample and reach the detector (4 m sample-to-detector distance) with a time stamp. Based upon the time-of-flight from the moderator to the detector (t_{tof}), moderator-to-detector (L_m), Planck's constant (h) and neutron mass (m_n) the wavelength (λ) of the neutron can be defined by $\lambda = (t_{tof}h)/(m_nL_m)$. The scattering vector (Q) is $Q = (4\pi/\lambda)\sin(\theta/2)$, where θ is the scattering angle. Data were placed on an absolute intensity scale via secondary standard, detector sensitivity and element size, sample transmission, and sample scattering volume considerations. Details regarding data collection and reduction can be found elsewhere (7). The neutron flux combined with a broad Q -range measured without changes in sample-to-detector distances is ideal for kinetic studies. The data may be reduced by a sequence of scripts to reconstruct kinetics within any defined time interval and sequence. This becomes critical when matching data with the predefined multi-step potential scans.

The eSANS working electrode was 80 pores per inch ($\approx 300 \mu\text{m}$ radius macropores) reticulated vitreous carbon (Electrosynthesis Inc.) cut to dimensions $3.8 \text{ cm} \times 1.2 \text{ cm} \times 0.4 \text{ cm}$ and fit within the center of a 4 mm path quartz spectroscopic cuvette (Starna), a Ag/AgCl in 3 mol/L KCl reference electrode (Microelectrodes, Inc) and platinum wounded thin wire counter electrode (Aldrich), separated from the working electrode by dialysis tubing.

A Series G 750 potentiostat (Gamry Instruments) was connected to a laptop via PCI expansion unit. A multi-step working electrode potential sequence was programmed from -0.3 V to -1.5 V in decrements of -0.1 V followed by a reverse scan from -1.4 V to -0.2 V in 0.2 V steps. In both the forward and reverse step scan a 5 s delay was applied to allow capacitance charge equilibration, followed by a 20 min chronocoulometry scan. Data were collected for each electrode step-profile and the measured current and synchronized with the SANS data collection. The sample environment was isolated from the user-operation hutch, therefore a remote method of communication between the sample and operations was devised by using a master laptop connected by wireless signal to the laptop that operates the potentiostat. The potentiostat was connected to the eSANS cell via short electrical cables passing through feed-ports at the sample enclosure. This approach proved necessary to check the signal integrity separately and remotely.

Results and Discussion

In order to develop eSANS into an analytical technique to measure the size of solution-dispersed nanoparticles during a redox reaction several criteria needed to be satisfied. The working electrode requires high conductivity, high surface area, and should not reduce the solvent of choice. For neutron scattering in a transmission mode, the working electrode must be of low neutron absorbance, low incoherent scattering, and have low scattering with the ability to contrast match. Contrast matching is a method by which the neutron refractive index of the solution is matched to the material such that no scattering contrast is present and therefore suppressed scattering signal (8). In the present work we

use a vitreous carbon electrode, as described previously (5), with a high degree of mm-to- μm porosity leading to high surface area. The sp^2 carbon hybridization leads to the high intrinsic conductivity and no incoherent scattering contribution that primarily arises from the presence of protons. In our approach, the electrodes are directly in the beam and may be contrast matched to the solvent as a mixture of 74.5 % D_2O and 25.4 % H_2O , by volume. However, in D_2O there is a scattering contribution that must be subtracted (5). In the three-terminal eSANS cell the platinum counter electrode and Ag/AgCl reference electrode are positioned outside of the passing neutron beam and therefore not exposed to any radiation (5). This assures that the dispersion that wets the porous vitreous carbon is the only analyte contributing to the scattering.

Electrochemical Small-Angle Neutron Scattering

The potential step sequence and SANS data acquisition were initiated simultaneously. **Figure 2a** shows the potential step sequence for the forward scan from -0.3 V in steps of -0.1 V to -1.5 V and then a reverse scan in increments of $+0.2$ V back to -0.2 V (not shown). In the current readout the marked downward spikes are due to the 5 s electrode charge capacitance equilibration step that occurs just after each potential step. After this equilibration the change in current signal due to each potential step can be observed. The maximum plateau current on the forward scan appears between -1.0 V and -1.2 V. Vitreous carbon electrodes do not reduce water under the potential step ranged used here; therefore the reactions we observe electrochemically are attributed to the dispersed ZnO nanoparticles and potentially oxygen reduction. In order to minimize the latter, buffered solutions were degassed by bubbling argon for 40 min.

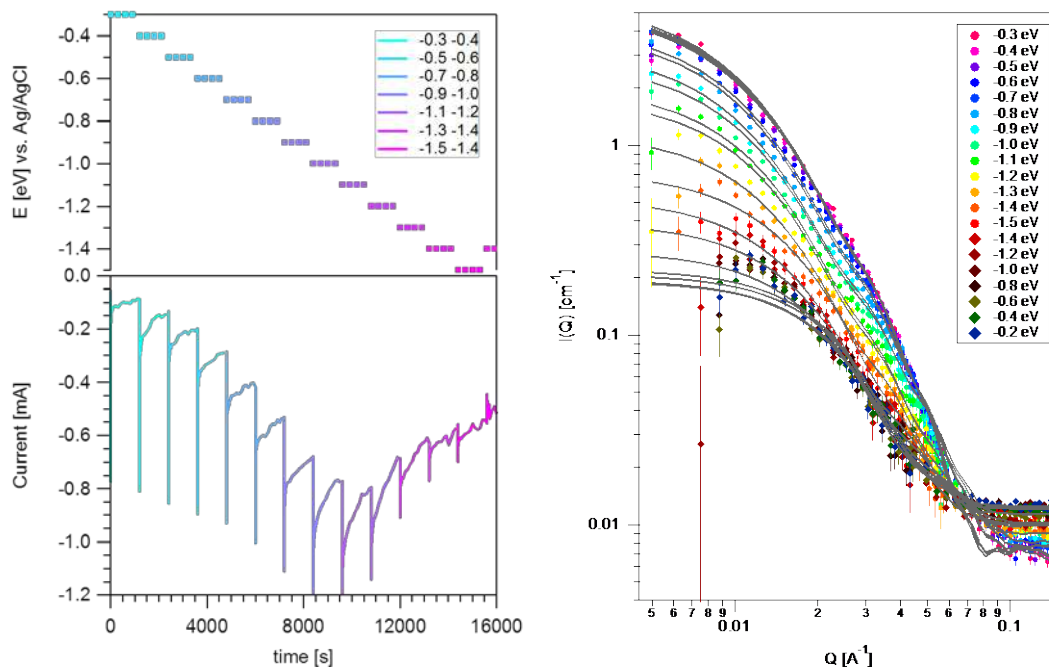


Figure 2. (a) Potential versus Ag/AgCl and measured current versus time in programmed steps from -0.3 V to -1.5 V and reverse scan. (b) eSANS data as a function of the electrode potential. Solid lines are the fits to the thin-disk with sticky-hard sphere structure factor.

The corresponding eSANS data are shown in **Figure 2b** from the forward and reverse scans after subtraction of a vitreous carbon electrode with deuterium oxide signal. The changes in scattering by the ZnO dispersions is indicative of an electrode potential

dependent change in solution structure on the nm scale. The analysis of the ZnO nanoparticles follows a model-approach to fit the scattering. A few salient details shall be provided.

SANS Modeling

Small-angle neutron scattering methods cover similar size scale ranges as small-angle X-ray scattering due to the sub-nm wavelengths (λ) used. The major difference is in the fundamental interaction between the waves and medium. X-rays are scattered by electrons and neutrons are scattered by the nuclei. For X-rays the atomic number is proportional to the scattering power, whereas with neutrons it is the atomic scattering length. The atomic scattering length varies from element to element which gives advantages in using neutron over X-ray scattering, especially with lower atomic number elements (such as C,H,D,O,N) that comprise many polymers. The contrast or scattering length density difference between solute and solvent may be changed by isotopic labeling due to the large coherent scattering length difference that occurs between hydrogen ($b_H = -0.374 \times 10^{-12}$ cm) and deuterium ($b_D = 0.667 \times 10^{-12}$ cm) isotopes. The scattering length density is quantified by $\rho = \sum b_i / v$, where the sum is over all atomic scattering lengths within molar volume, v . SANS contrast may be enhanced with isotopic substitution by using deuterium oxide as the solvent with organic and inorganic solutes.

Analysis of the scattered intensity versus wave vector was conducted by using the form factor, $P(Q)$, of a thin disk and a sticky-hard sphere structure factor, $S(Q)$, that accounts for pair-wise attractive interactions, and background, I_{inc} , arising from incoherent scattering contributions. Eq. 1 shows that the scattering is proportional to concentration of nanoparticles C_{NP} , square of the nanoparticle geometric volume (V_{NP}), and scattering length density difference between nanoparticle (ρ_{NP}) and solvent (ρ_s). In this case, the scattering length density difference occurs between the ZnO nanoparticle ($\rho_{ZnO} = 4.76 \times 10^{-6} \text{ \AA}^{-2}$) and solvent, deuterium oxide ($\rho_s = 6.33 \times 10^{-6} \text{ \AA}^{-2}$).

$$I(Q) = (\rho_{NP} - \rho_s)^2 C_{NP} V_{NP}^2 P(q) S(q) + I_{inc} \quad [2]$$

The form factor for a thin disk is given by

$$P(Q, R, L) = \int_0^{\pi/2} \Psi(Q, R, L, \alpha)^2 \sin \alpha d\alpha \quad [3]$$

Where, the analytic expression for the amplitude $\Psi(Q, R, L, \alpha)$ is given by

$$\Psi(Q, R, L, \alpha) = \frac{2J_1(QR \sin \alpha)}{QR \sin \alpha} \frac{\sin(QL \cos \alpha / 2)}{QL \cos \alpha / 2} \quad [4]$$

and $J_1(x)$ is the first-order Bessel function of the first kind. The square of the amplitude was numerically integrated over all orientation angles α and R and L are the radius and thickness of the disk, respectively ⁽⁹⁾.

The structure factor, $S(Q)$, was modeled using a sticky-hard sphere (SHS) potential developed by Menon et al. (10). In this case a square-well potential of depth (u_0), hard-sphere diameter ($\sigma = 2R$) and well width (Δ) define the inter-particle potential. The structure factor accounts for the non-ideal solution through pair-wise interactions within the Ornstein-Zernike equation. These pair-wise attractive interactions improve the fit to

the experimental data. At the ionic strength used the long-range electrostatic interactions are screened and weaker van der Waals forces provide the attraction by the SHS model, since these nanoparticles are not steric-stabilized by polymers.

Each electrode potential dependent $I(Q)$ dataset were fit for R, L, C_{NP} , SHS parameter, and I_{inc} with fixed values for ρ_{NP} , ρ_s , and Δ by Levenberg-Marquardt non-linear least squares regression routines that minimized the chi-squared statistic between model and experiment using the associated experimental uncertainties (9). Uncertainties (error bars) are estimated by one standard deviation of the mean by least-squares minimization of fits to the eSANS data. While error bars are shown, they may be smaller than the symbols used in some cases. **Figure 2b** shows the curve fit for each data set. **Figure 3a** shows the main results of the particle radius decreasing upon increased negative electrode potential with minor dependence on the total disk thickness (**Figure 3b**). At the first few potential steps there is no change in eSANS data therefore we do not expect any change in size, however, that would not exclude redox or electron transfer taking place, simply no particle-scale structure changes. As shown in **Figure 3a**. The radius remains essentially unchanged from -0.3 V to -0.9 V then the radius decreases monotonically to $12.8 \text{ nm} \pm 3 \text{ nm}$ at -1.5 V, then upon the reverse scan the radius continues to decrease and plateau in size near -1.0 V with no further change. The ZnO disk thickness shows very little change during the forward and reverse scans.

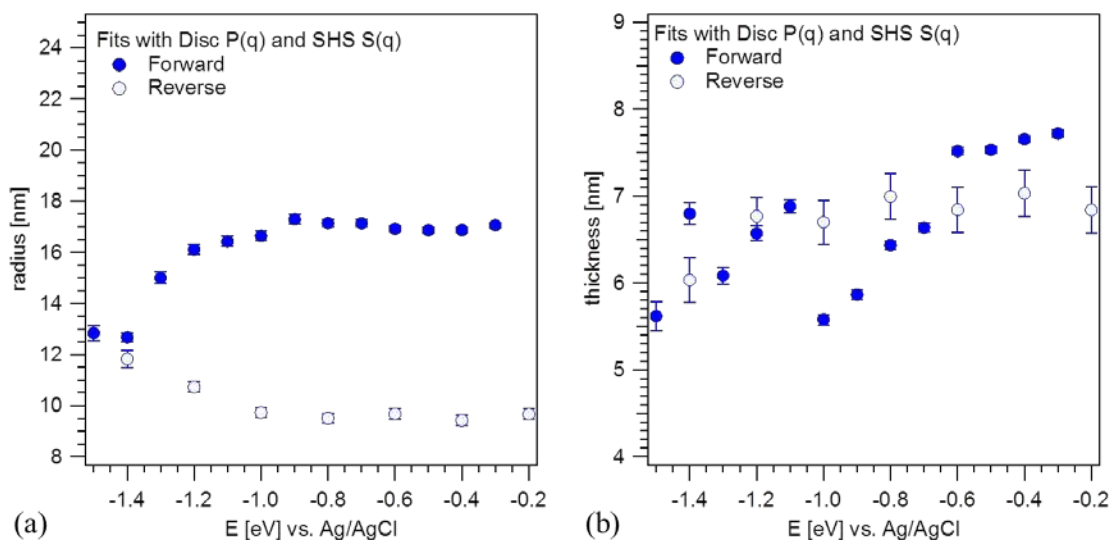


Figure 3. eSANS data fit by disk form factor and attractive sticky hard sphere structure factor: (a) Radius and (b) thickness versus sampled electrode potential (versus Ag/AgCl) for scan from -0.3 to -1.5 V and reverse scan. Each data point is an average over the final 2 min of the 20 min potential step scan.

Chronocoulometry Modeling

The eSANS data show a decrease in ZnO nanoparticle average size as a function of negative electrode potential. The particles in these dispersions must rely on diffusion to the electrode for the electron transfer and redox reaction to occur in the absence of mobile reducing agents or prior adsorption to the electrode. In order to provide insight into the redox kinetics, the current (**Figure 4**) was modeled (4) with a one-dimensional, irreversible reaction-diffusion process of **Eq. 5** where t is the time after the initial potential step at time t_0 , C_0 is the initial concentration of species, A active electrode area,

k_f the forward reaction rate constant, D_o is the oxidized species diffusivity that equals the reduced species diffusivity (D_R) and $\Gamma = k_f^2/D_o$. In this model, convective and drift contributions are not considered.

$$i_{ir}(t - t_0) = F A k_f C_o e^{\Gamma(t-t_0)} \operatorname{erfc}\left(\sqrt{\Gamma(t-t_0)}\right) \quad [5]$$

The forward rate constant follows the activated process form $k_f \approx \exp(E - E^{\circ})$, where E° is the standard reduction potential and E is the electrode potential. **Eq. 5** was independently fit to each chronocoulometry scan as a function of potential step shown in **Figure 4**, excluding the charge capacitance equilibration duration. The main results are in **Figure 5** where the eSANS measured particle radius and lumped parameters ($F A k_f C_o$) and Γ are plotted as a function of E . In **Figure 5a** a forward scan broad peak in $F A k_f C_o$ near -1.1 V occurs near the midpoint of the change in particle size due to reduction and near the value for the bulk reduction of Zn^{2+} to Zn^0 of -1.26 V. This implies a maximum in the forward rate constant, since the product of $F A C_o$ is expected to be constant. However, as the reaction proceeds beyond -1.2 V the reduction rate ($F A k_f C_o$) decreases. This kinetic decrease is also observed in Γ that provides insight into the ratio of the forward reaction rate to the diffusivity as shown in **Figure 5b**.

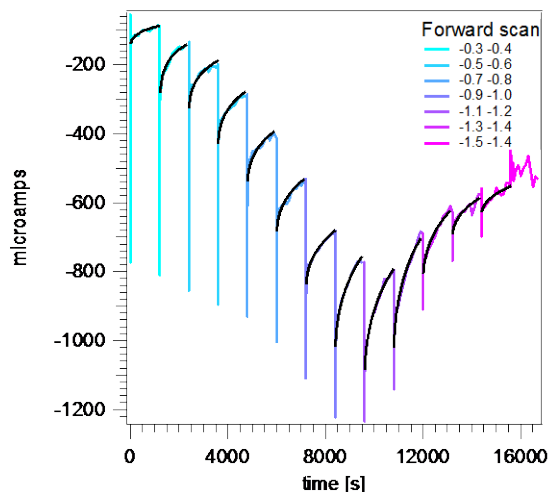


Figure 4. Semi-infinite, linear diffusion current governed by mass transfer and irreversible charge transfer kinetics fit to ZnO in 25 mmol/L pH 7 potassium phosphate buffer chronocoulometry data as a function of the sequential electrode potential steps. Fits appear after capacitance charge equilibration and within each 0.1 V potential step.

The peak in Γ between -0.9 V and -1.5 V is consistent with a reduced forward reaction rate at negative potentials and above the expected bulk reduction potential for ZnO. While the model assumes D_o is constant the particle size decreases, so the diffusivity would increase and also contribute to a reduced Γ at negative potentials. Therefore the lowering of Γ at negative potentials on the forward scan is indicative of a mechanism to reduced reaction rate within the electrode-surface region. In the eSANS approach, the total scattering is measured. The only additional insight provided remains in the analysis of the structure factor, $S(Q)$. The SHS results shows that the nanoparticle attraction increases with negative potentials, so the association or aggregation of particles also contributes and is beyond the scope presented here. The nanoparticle structure at the

electrode surface region is directly testable by alternative experimental methods rather than the ones devised here, such as neutron and X-ray reflectivity.

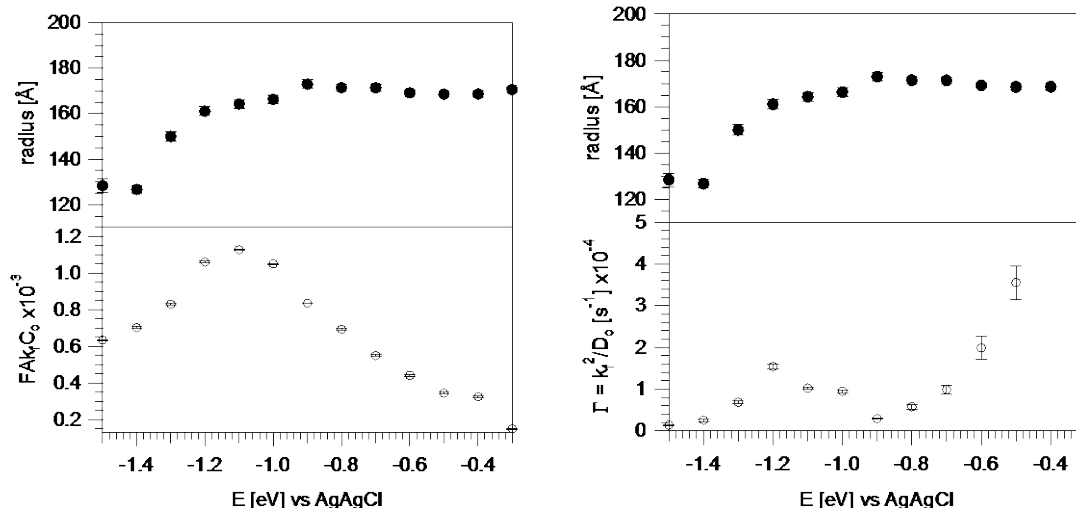


Figure 5. (a) $F\Delta k_f C_o$ and (b) $\Gamma = k_f^2/D_o$ and radius in top versus sampled electrode potential (versus Ag/AgCl) for scan from -0.3 V to -1.5 V for ZnO nanoparticles in 25 mmol/L pH 7 deuterium oxide phosphate buffer.

Structure–reaction hypothesis

As a ZnO nanoparticle undergoes reduction two extreme transformation cases could be considered: a uniform reduction and dissolving shell upon reduction. The scattered intensity to zero angle $I(0)$ is a product of the square of the contrast factor, concentration of the particles, and square of the volume of the particles by **Eq. 2**. In the case a particle uniformly reduces from ZnO to Zn then the scattering length density would vary as a function of the redox extent because the elemental composition changes by the elimination of oxygen. However, in a dissolving, reduced shell the particle contrast is a constant and only the size changes. These two opposing physical models were calculated and compared as a function of redox extent of the particle in **Figure 6**.

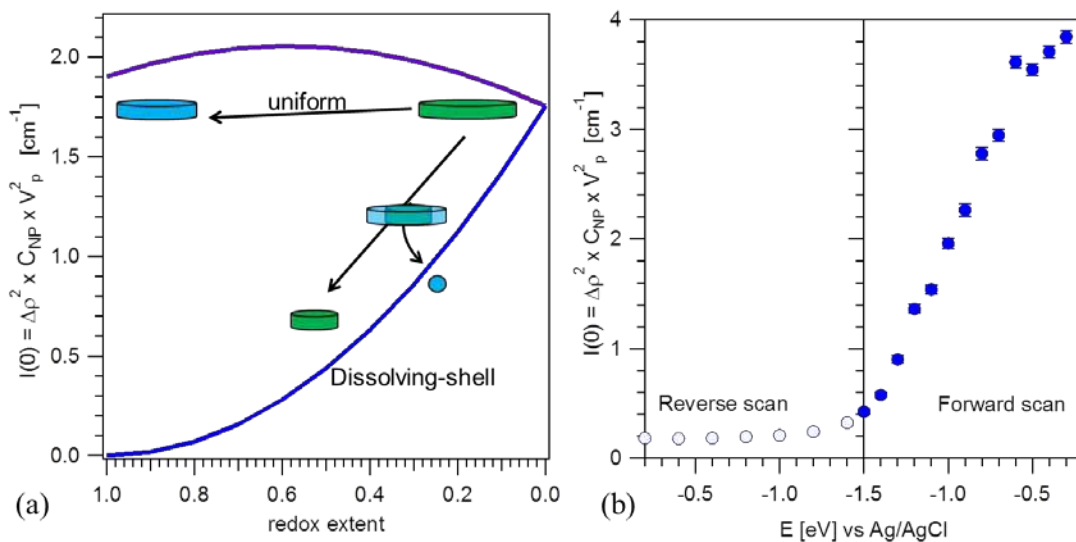


Figure 6. Variation in $I(0)$ for (a) model as a function of redox extent and (b) eSANS experiment. The monotonic change in the $I(0)$ with forward reaction is consistent with a dissolved–shell mechanism, rather than a uniform particle reduction.

The uniform reduction where ρ_{NP} of the particle changes from pure ZnO ($\rho_{\text{ZnO}} = 4.76 \times 10^{-6} \text{ \AA}^{-2}$) to Zn ($\rho_{\text{Zn}} = 3.74 \times 10^{-6} \text{ \AA}^{-2}$) as a function of redox extent as well as the particle volume is due to the combined effect of a loss of oxygen and a change in mass density. Assuming no change in particle concentration the expected $I(0)$ has a broad maximum as a function of redox extent. The dissolving shell model has a constant particle ρ_{NP} and as the redox extent increases the particle volume decreases and the reduced shell dissolves leaving a monotonically reduced particle volume. This model (**Figure 6a**) leads to a monotonically decreasing $I(0)$ with constant concentration. Comparison of these two predictions with the model-independent analysis of $I(0)$ in **Figure 6b**, the data are consistent with the dissolving-shell picture as in the forward scan there is a reduced $I(0)$ that continues and plateaus during the reverse scan. While there is not a direct correspondence between the model redox extent and the electrode potential, the model independent approach aids in SANS form factor $P(Q)$ analysis.

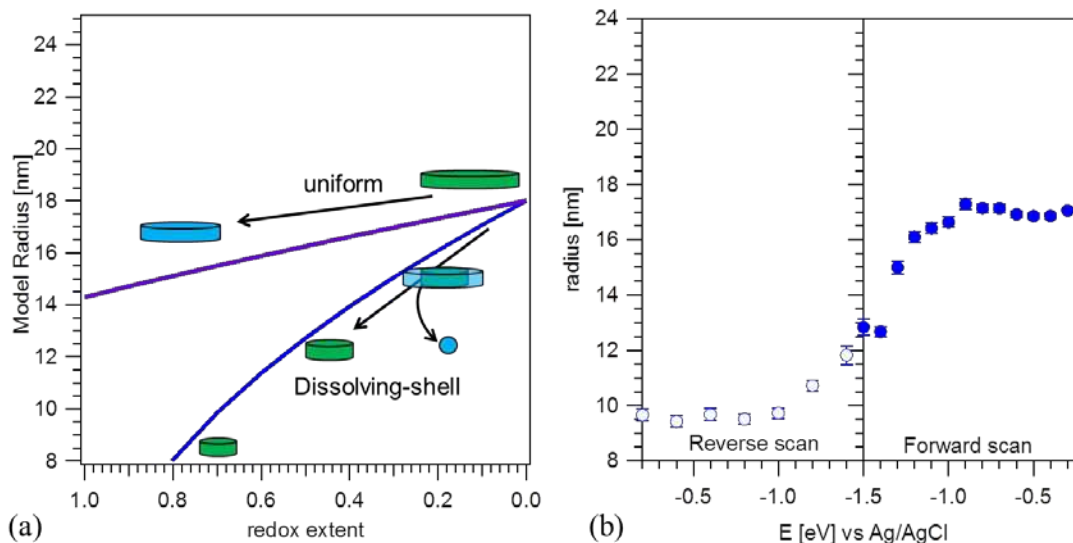


Figure 7. Variation in radius with (a) model redox extent and (b) eSANS experiment.

The same model was applied to show two extremes in the ZnO radius as a function of redox extent. **Figure 7a** shows the magnitude in change in size under complete reduction for uniform and dissolving shell, whereas the experimental data are provided in **Figure 7b** that assumed a constant nanoparticle composition and scattering length density of pure ZnO.

Conclusions

The size and pair-wise particle interaction sensitivity provided by small-angle neutron scattering was combined with electrochemical methods to develop an electrochemical SANS technique. This method was applied to follow the size and interactions of zinc oxide nanoparticle dispersions as a function of reduction at the vitreous carbon electrode. eSANS finds an irreversible-shell dissolution mechanism occurs upon negative electrode potentials. The chronocoulometry analysis shows the reaction rate reaches a maximum with reduced rate at negative potentials. This implies a structuring at the electrode-interface structure causes a reduced reaction rate for these dilute dispersions. The attractive interactions between ZnO particles accounted for by the sticky-hard sphere model are hypothesized to be responsible for this reaction slow-down.

This transmission eSANS method probed a well-defined Pourbaix diagram and offers the possibility to follow polymer-nanoparticle complexes by the use of contrast variant neutron scattering methods.

Acknowledgments

We acknowledge the Center for Nanophase Materials Sciences and Spallation Neutron Source user program, proposal CNMS2011-125 at Oak Ridge National Laboratory sponsored by the Scientific User Facility Division, Office of Basic Energy Sciences, and U.S. Department of Energy.

Certain commercial equipment and materials are identified in this paper in order to specify adequately the experimental procedure. In no case does such identification imply recommendations by the National Institute of Standards and Technology nor does it imply that the material or equipment identified is necessarily the best available for this purpose.

*Official contribution of the National Institute of Standards and Technology; not subject to copyright in the United States

References

1. E.Frohlich,C.Samberger,T.Kueznik,M.Absenger,E.Roblegg,A.Zimmer and T.R.Pieber, *Journal of Toxicological Sciences*, **34**(4), 363-375 (2009).
2. P.J.Moos,K.Chung,D.Woessner,M.Honeggar,N.S.Cutler and J.M.Veranth, *Chemical Research in Toxicology*, **23**(4), 733-739 (2010).
3. S.Ostrovsky,G.Kazimirsky,A.Gedanken and C.Brodie, *Nano Research*, **2**(11), 882-890 (2009).
4. A.J.Bard and L.R.Faulkner *Electrochemical Methods Fundamentals and Applications*, John Wiley & Sons, Inc.: Hoboken, New Jersey, (2001).
5. V.M.Prabhu and V.Reipa, *Journal of Physical Chemistry Letters*, **3**(5), 646-650 (2012).
6. B.Beverskog and I.Puigdomenech, *Corrosion Science*, **39**(1), 107-114 (1997).
7. J.K.Zhao, *Nuclear Instruments & Methods in Physics Research Section A-Accelerators Spectrometers Detectors and Associated Equipment*, **647**(1), 107-111 (2011).
8. Higgins, J. S. and Benoit, H. C. *Polymers and Neutron Scattering*, Oxford University Press, Inc.: New York, (2002).
9. S.R.Kline, *Journal of Applied Crystallography*, **39**, 895-900 (2006).
10. S.V.G.Menon,C.Manohar and K.S.Rao, *Journal of Chemical Physics*, **95**(12), 9186-9190 (1991).